iScience

CellPress
OPEN ACCESS

Article

Sex differences in left-ventricular strain in a murine model of coxsackievirus B3 myocarditis

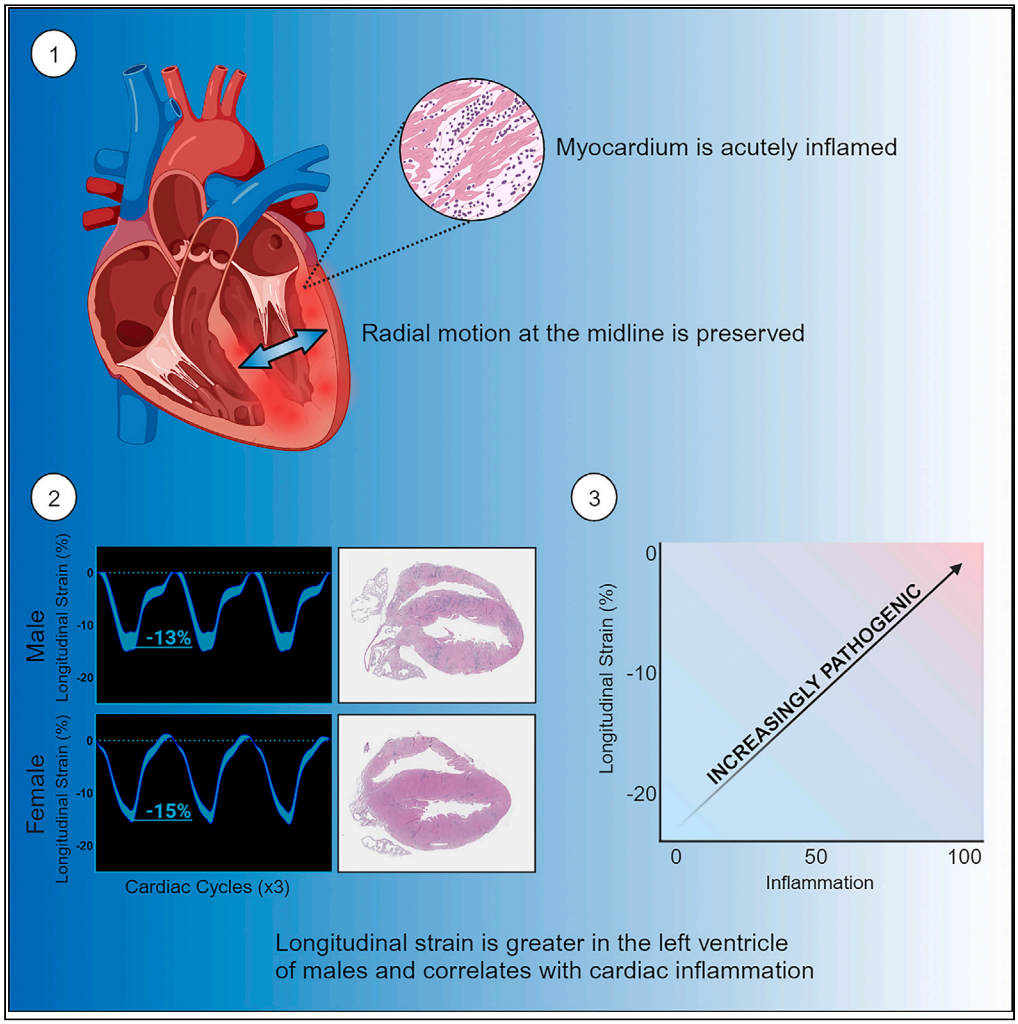

Damian N. Di Florio, Logan P. Macomb, Presley G. Giresi, ..., Chris J. McLeod, Mohamad H. Yamani, DeLisa Fairweather

Fairweather.DeLisa@mayo.edu

Highlights

Radial motion at the mid-left ventricle is preserved during acute myocarditis

Longitudinal strain is worse in males with myocarditis compared to females

Cardiac inflammation and longitudinal strain are correlated

Di Florio et al., iScience 26, 108493
December 15, 2023
https://doi.org/10.1016/j.isci.2023.108493

iScience

CellPress
OPEN ACCESS

Article

Sex differences in left-ventricular strain in a murine model of coxsackievirus B3 myocarditis

Damian N. Di Florio,[1,2,3] Logan P. Macomb,[1] Presley G. Giresi,[1] Danielle J. Beetler,[1,2,3] Natalie E. Bonvie-Hill,[1] Katie A. Shapiro,[1] Abdel-Rahman N. Naser,[1] Sami Khatib,[1] Emily R. Whelan,[1,2,3] Gabriel J. Weigel,[1] Brandy H. Edenfield,[4] Varsini Balamurugan,[1] Sarah K. Burris,[5] Laurie J. Rich,[5] Katelyn A. Bruno,[1,6] Leslie T. Cooper, Jr.,[1] Chris J. McLeod,[1] Mohamad H. Yamani,[1] and DeLisa Fairweather[1,2,7,8,9,*]

SUMMARY

Myocarditis is typically caused by viral infections, but most cases are thought to be subclinical. Echocardiography is often used for initial assessment of myocarditis patients but is poor at detecting subtle changes in cardiac dysfunction. Cardiac strain, such as global longitudinal strain (GLS) and global circumferential strain (GCS), represents an increasingly used set of measurements which can detect these subtle changes. Using a murine model of coxsackievirus B3 myocarditis, we characterized functional changes in the heart using echocardiography during myocarditis and by sex. We found that 2D GLS, 4D mode, and 4D strains detected a significant reduction in ejection fraction and GLS during myocarditis compared to baseline and in males compared to females. Furthermore, worse GLS correlated to increased levels of CD45$^+$, CD11b+, and CD3$^+$ immune cells. Our findings closely resemble published reports of GLS in patients with myocarditis indicating the usefulness of this animal model for translational studies of myocarditis.

INTRODUCTION

Myocarditis is defined as myocardial inflammation and can lead to sudden cardiac death, heart failure, and progress to dilated cardiomyopathy (DCM) in susceptible individuals.[1–3] However, most cases of myocarditis (i.e., lymphocytic) are relatively mild. Echocardiography is often used to determine cardiac function prior to a diagnosis of myocarditis, especially in smaller regional centers where a cardiac MRI (CMR) is not available. Traditional echocardiography has a poor ability to detect cardiac dysfunction in patients with myocarditis unless the patient has severe myocarditis (i.e., fulminant) or develops a dilated phenotype (i.e., DCM). In the past several years global longitudinal strain (GLS) derived from echocardiography or CMR has been used to more accurately detect cardiac dysfunction in patients with myocarditis.[4–10] In contrast, animal models of myocarditis often report cardiac dysfunction using 2D M-mode echocardiography because this modality is more often available to researchers.[11,12]

Studies of sex differences in myocarditis indicate that more males than females die of myocarditis worldwide.[13] Clinical studies of myocarditis in the past decade consistently report a sex ratio of 2–4:1 male to female.[14–20] Additionally, myocarditis occurs most frequently in men under age 50 and especially from age 16–30 whereas women are at a greater risk of developing myocarditis after age 50 (i.e., postmenopause).[14,15,17,18,20] We utilize a translational autoimmune mouse model of viral myocarditis where a mild infection of heart-passaged coxsackievirus B3 (CVB3) leads to acute myocarditis at day 10 post infection and progresses to DCM around day 35.[21–23] Sex differences in the immune response during CVB3 myocarditis in mice have been well described (reviewed in Fairweather et al.[14,24]). This animal model is highly translational with similar findings for mice and humans for a number of markers including a dominant infiltrate of macrophages with fewer T cells,[4,17,25] serum biomarkers (i.e., sST2, myoglobin, miR-721),[17,26–28] complement receptors (i.e., CD11b/CR3),[29–31] TLR4/IL-1β/inflammasome,[32–35] and Th17 expression,[36] for example.

The goal of this study was to assess the ability of various echocardiography imaging techniques including 4D to detect cardiac dysfunction in this murine model of viral myocarditis, according to sex. This is essential due to the high utility of this animal model in providing preclinical assessments of the pathogenesis of disease as well as novel biomarkers and therapies for myocarditis and DCM.

[1]Department of Cardiovascular Medicine, Mayo Clinic, Jacksonville, FL, USA
[2]Center for Clinical and Translational Science, Mayo Clinic, Rochester, MN, USA
[3]Mayo Clinic Graduate School of Biomedical Sciences, Mayo Clinic, Rochester, MN, USA
[4]Department of Cancer Biology, Mayo Clinic, Jacksonville, FL, USA
[5]Fujifilm VisualSonics Inc, Toronto, ON, Canada
[6]Division of Cardiovascular Medicine, Department of Medicine, University of Florida, Gainesville, FL, USA
[7]Department of Immunology, Mayo Clinic, Jacksonville, FL, USA
[8]Department of Medicine, Mayo Clinic, Jacksonville, FL, USA
[9]Lead contact
*Correspondence: Fairweather.DeLisa@mayo.edu
https://doi.org/10.1016/j.isci.2023.108493

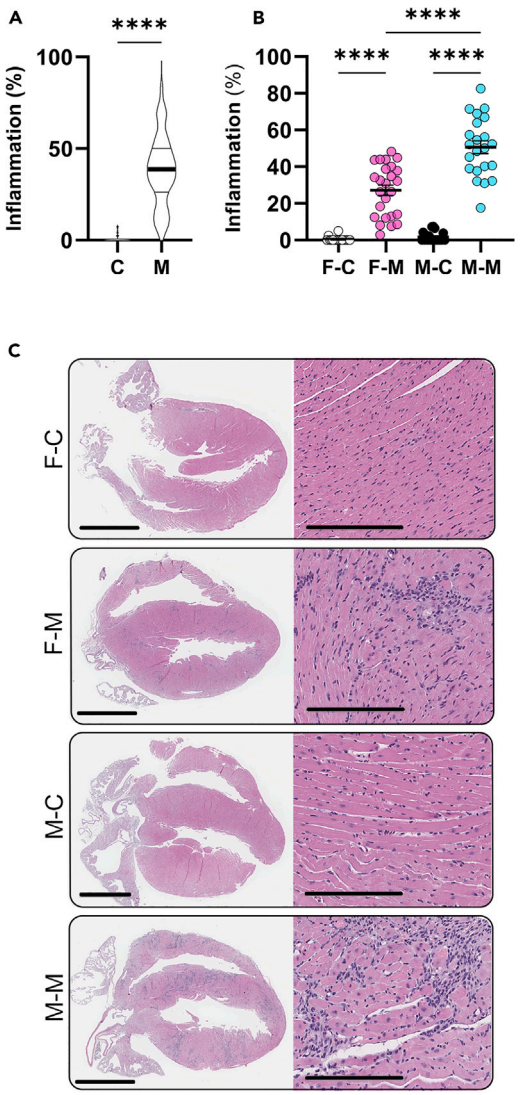

Figure 1. Males develop worse myocarditis compared to females

(A) Myocarditis severity (Inflammation %) between male (M) and female (F) uninfected controls (C, n = 37) and myocarditis (M, n = 47) (unpaired t-test; violin plots depict mean and interquartile range); (B) Myocarditis severity by sex: F-C (n = 17), F-M (n = 23), M-C (n = 20), M-M (n = 22) (one-way ANOVA with Tukey's multiple comparison test; scatterplots show mean ± SEM); (C) Representative heart sections (scale bars, 2 mm and 200 μm for low and high-power images, respectively). A, B ****$p < 0.0001$.

RESULTS

Males develop worse myocarditis than females

To confirm sex differences in our model of viral myocarditis we compared male and female mice with myocarditis to controls at day 10 after infection. Cardiac inflammation was significantly increased compared to controls ($p < 0.0001$) (Figure 1A) and in males compared to females with myocarditis (ANOVA $p < 0.0001$, males vs. females $p < 0.0001$) (Figure 1B). Representative images are shown in Figure 1C.

We examined individual immune cell markers during myocarditis using immunohistochemistry by sex. As expected males with myocarditis had significantly more expression of CD45 (all immune cells) (ANOVA $p < 0.0001$; males vs. females $p = 0.0002$) (Figure 2A), CD11b (activated neutrophils, macrophages, mast cells, and some dendritic cells) (ANOVA $p < 0.0001$; males vs. females $p = 0.0008$) (Figure 2B), F4/80 macrophages (ANOVA $p < 0.0001$; males vs. females $p = 0.025$) and CD3 (all T cells) (ANOVA $p < 0.0001$; males vs. females $p = 0.002$) (Figure 2C) compared to females with myocarditis.

Additionally, as expected males have higher heart weight compared to females ($p < 0.0001$) even after controlling for body size with tibia length ($p < 0.0001$) (Figure 3), which can affect echocardiography data.

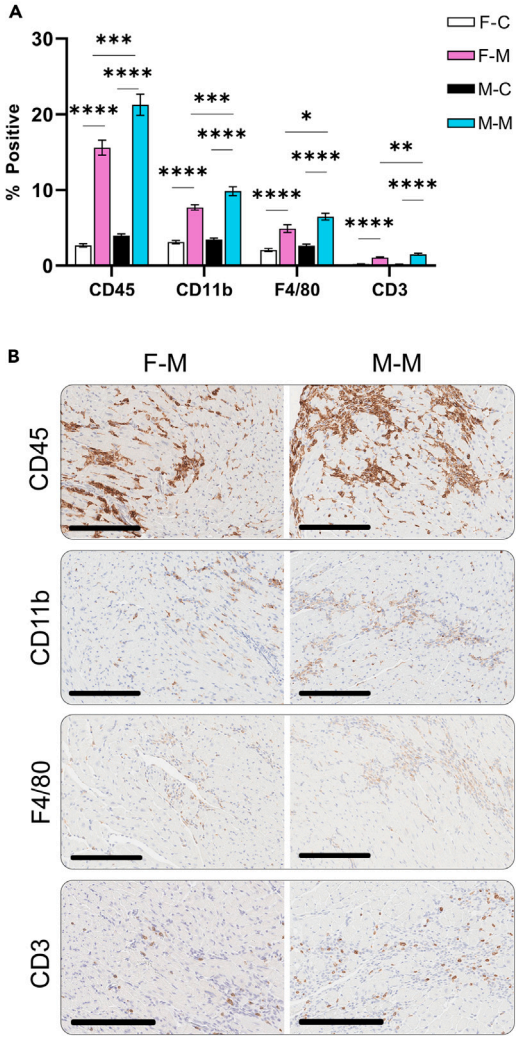

Figure 2. Proinflammatory markers are increased in male hearts during myocarditis

(A) Percent positive staining of mouse myocardium controls (F-CON n = 17, M-CON n = 19) and myocarditis (F-M n = 25, M-M n = 22; bar graphs show mean ± SEM) with (B) representative images for CD45, CD11b, F480, and CD3 (scale bars, 200 μm). One-way ANOVA with Tukey's multiple comparison tests for each immune marker. (A) **p < 0.01, ***p < 0.001, ****p < 0.0001.

Traditional 2D M-mode echocardiography during myocarditis

Echocardiography assessments of myocarditis in the literature often use 2D short axis motion (M)-mode of the left ventricle (LV)[11,12] and we used this traditional method to compare mice with myocarditis to baseline controls and by sex (Figure 4). Mice with myocarditis had significantly lower heart rates compared to baseline (p < 0.0001) (Figure 4A). Decreased heart rate can affect echocardiography parameters that are normalized per unit time (i.e., cardiac output (CO) expressed as μL/min). A heart rate of 350–450 bpm is generally possible in healthy animals; however, mice with myocarditis have decreased heart rate under the same anesthetic conditions.

Mice with myocarditis had significantly decreased stroke volume (p = 0.004) (Figure 4F), CO (p < 0.0001) (Figure 4G), and LV mass/corrected LV mass (both p < 0.0001) (Figures 4J and 4K); however, other key functional parameters like LV ejection fraction (LVEF) (p = 0.08) were not significantly different (Figures 4B–4D and 4H). Measurements that describe wall thickness during contraction and relaxation were all found to be significantly reduced during myocarditis demonstrating reduced contractility (Figures 4N and 4O). When we examined sex differences in myocarditis, 2D M-mode only identified worse LV end diastolic diameter (LVEDD) (p = 0.03) and LV end diastolic volume (LVEDV) (p = 0.03) in males compared to females (Table 1).

4D-mode reveals worse LVEF during myocarditis, but no sex differences

M-mode echocardiography is limited to a single plane, so volumes are estimated and may not represent the geometry of the entire ventricle. To determine whether measurements improve by increased sampling of the entire LV (i.e., volume) we used 4D-mode (3D in motion). We

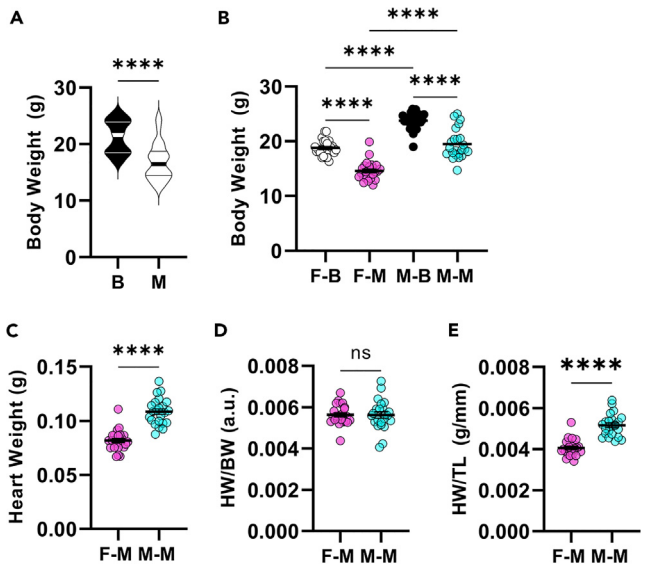

Figure 3. Males have higher heart weight than females during myocarditis

(A) Body weight of mice at baseline (B, n = 50) compared to myocarditis (M, n = 48) (violin plots depict mean and interquartile range); (B) scatterplots show change in body weight for F-B (n = 25), M-B (n = 25), F-M (n = 25) and M-M (n = 23); C, heart weight (HW); (D) HW/BW ratio (arbitrary units = a.u.); (E) HW/tibia length (HW/TL) (scatterplots show mean ± SEM); (A–E) ****p < 0.0001.

found a significant decrease in LVEF (p = 0.001), stroke volume (p = 0.0007), CO (p < 0.0001), and dV/dT (rate of change of LV volume) (p < 0.0001) during myocarditis compared to baseline (Figures 5A, 5D, 5E, and 5F). Although 4D volume analysis of males and females at baseline revealed significant differences in several parameters (Figures 5H–5L), sex differences were not observed during myocarditis (Figures 5M–5R).

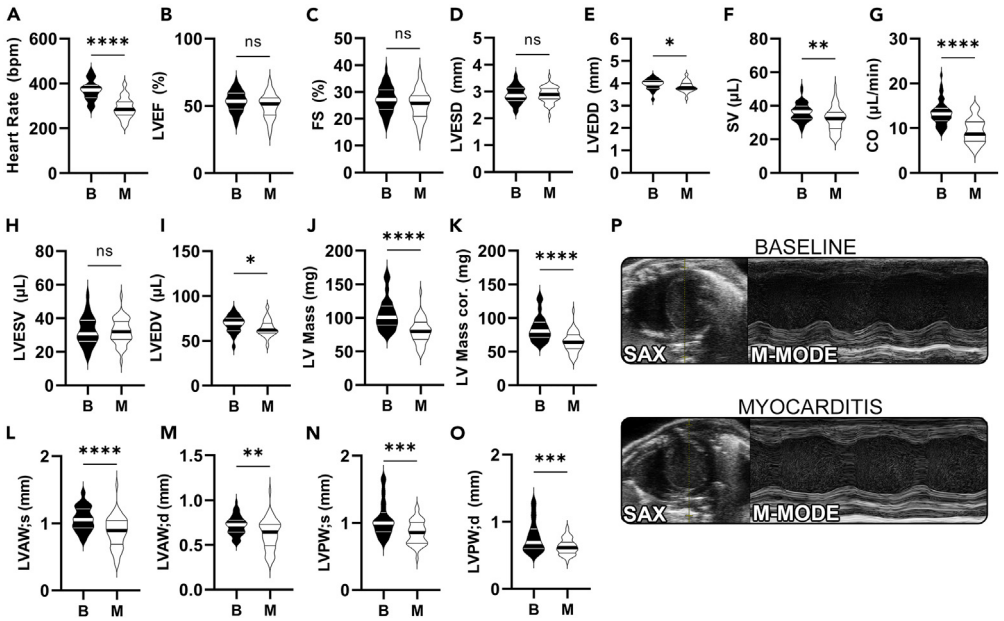

Figure 4. Traditional 2D M-mode shows no difference in LVEF during myocarditis

(A–O) Standard LV motion (M)-mode parameters comparing female and male mice at baseline (B, n = 44) compared to myocarditis (M, n = 42) (unpaired t-test; violin plots depict mean and interquartile range); (P) representative short-axis (SAX) and M-mode images at baseline and during myocarditis. Abbreviations: CO, cardiac output; FS, fractional shortening; LVAW; d, LV anterior wall thickness at diastole; LVAW; s, LV anterior wall thickness at systole; LVEDD, LV end diastolic diameter; LVEDV, LV end diastolic volume; LV, left ventricular; LVEF, LV ejection fraction; LVESD, LV end systolic diameter; LVESV, LV end systolic volume; LVPW; d, LV posterior wall thickness at diastole; LVPW; s, LV posterior wall thickness at systole; SV, stroke volume. (A–O) *p < 0.05, **p < 0.01, ***p < 0.001 ****p < 0.0001.

Table 1. Left-ventricular motion mode echocardiography by sex

	F-B (n = 21)[a]	M-B (n = 21)	p	F-M (n = 22)	M-M (n = 20)	p
Heart Rate (bpm)	369.0 (45.0)[b]	370.4 (44.6)	0.907	299.1 (46.4)	280.8 (43.3)	0.244
LVEF (%)	55.84 (6.55)	50.38 (8.19)	**0.014**[c]	51.09 (9.65)	48.84 (8.71)	0.575
FS (%)	28.78 (4.22)	25.51 (5.17)	**0.014**	25.87 (6.04)	24.48 (5.14)	0.627
LVESD (mm)	2.74 (0.27)	3.04 (0.30)	**0.002**	2.80 (0.30)	2.97 (0.25)	0.110
LVEDD (mm)	3.84 (0.25)	4.08 (0.15)	**0.0005**	3.78 (0.24)	3.93 (0.21)	**0.030**
SV (μL)	35.55 (5.97)	36.72 (4.78)	0.485	31.26 (7.25)	32.93 (7.47)	0.446
CO (μL/min)	13.10 (2.69)	13.65 (2.81)	0.485	9.37 (2.68)	9.35 (2.89)	0.911
LVESV (μL)	28.42 (6.80)	36.83 (8.69)	**0.002**	30.15 (7.69)	34.40 (7.06)	0.110
LVEDV (μL)	63.97 (9.50)	73.56 (6.71)	**0.0005**	61.40 (9.26)	67.33 (8.64)	**0.030**
LV Mass (mg)	96.98 (19.43)	115.7 (26.0)	**0.006**	78.00 (16.77)	82.63 (20.35)	0.172
LV Mass Corr. (mg)	77.58 (15.5)	92.5 (20.1)	**0.006**	62.4 (13.42)	66.10 (16.28)	0.172
LVAW;s (mm)	1.104 (0.18)	1.021 (0.18)	0.116	0.908 (0.23)	0.834 (0.24)	0.609
LVAW;d (mm)	0.725 (0.12)	0.709 (0.10)	0.642	0.635 (0.17)	0.607 (0.18)	0.999
LVPW;s (mm)	0.996 (0.22)	1.109 (0.28)	0.182	0.827 (0.16)	0.876 (0.18)	0.215
LVPW;d (mm)	0.727 (0.18)	0.825 (0.27)	0.376	0.624 (0.12)	0.635 (0.12)	0.699

[a]B, baseline; CO, cardiac output; F, female; FS, fractional shortening; LVAW; d, left ventricular anterior wall thickness at diastole; LVAW; s, left ventricular anterior wall thickness at systole; LVEDD, left ventricular end diastolic diameter; LVEDV, left ventricular end diastolic volume; LVEF, left ventricular ejection fraction; LVESD, left ventricular end systolic diameter; LVESV, left ventricular end systolic volume; LVPW, d, left ventricular posterior wall thickness at diastole; LVPW, s, left ventricular posterior wall thickness at systole; SEM, standard error of the mean; M, male or myocarditis; SV, stroke volume.
[b]Data are represented as mean ± SEM.
[c]Bolded p values indicate statistical significance for Mann-Whitney test.

4D strain reveals reduced LVEF during myocarditis and in males

Because 4D strain software requires higher quality images for accuracy, only a subset of the original dataset that had high image quality was used for this analysis. We examined traditional echocardiography endpoints using the 4D Strain software. Using this software, we found that

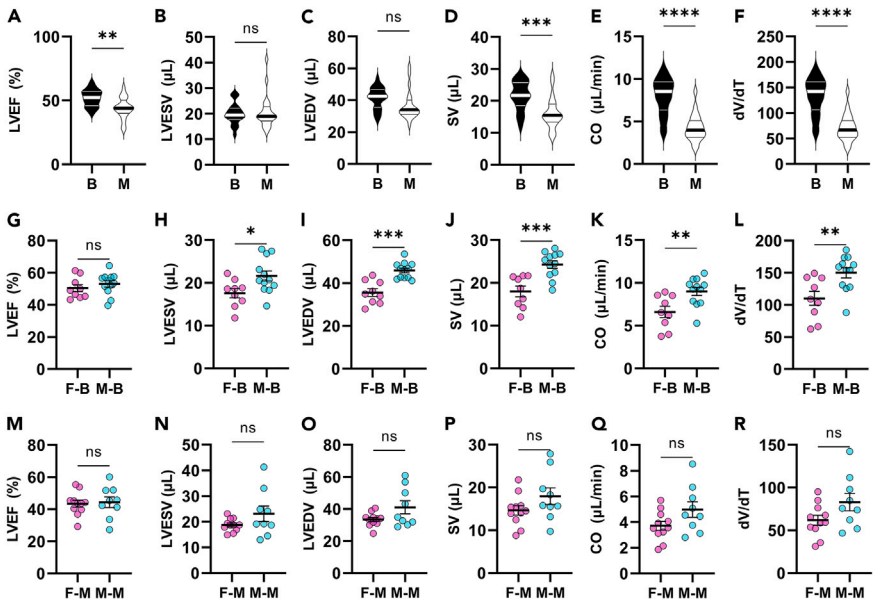

Figure 5. 4D mode LV parameters reveal worse myocarditis but no sex differences

(A–F) LV functional parameters from 4D mode compare mice at baseline (B, n = 21) to myocarditis (M, n = 20) (unpaired t-test; violin plots depict mean and interquartile range); (G–L) females (F-B) vs. males (M-B) at baseline (Mann-Whitney; scatterplots show mean ± SEM); (M–R) females (F-M) vs. males (M-M) during myocarditis (Mann-Whitney; scatterplots show mean ± SEM). Abbreviations: CO, cardiac output; dV/dT = rate of change of LV volume; LV, left ventricular; LVEDV, LV end diastolic volume; LVEF, LV ejection fraction; LVESV, LV end systolic volume; SV, stroke volume. (A–R) *p < 0.05, **p < 0.01, ***p < 0.001, ****p < 0.0001.

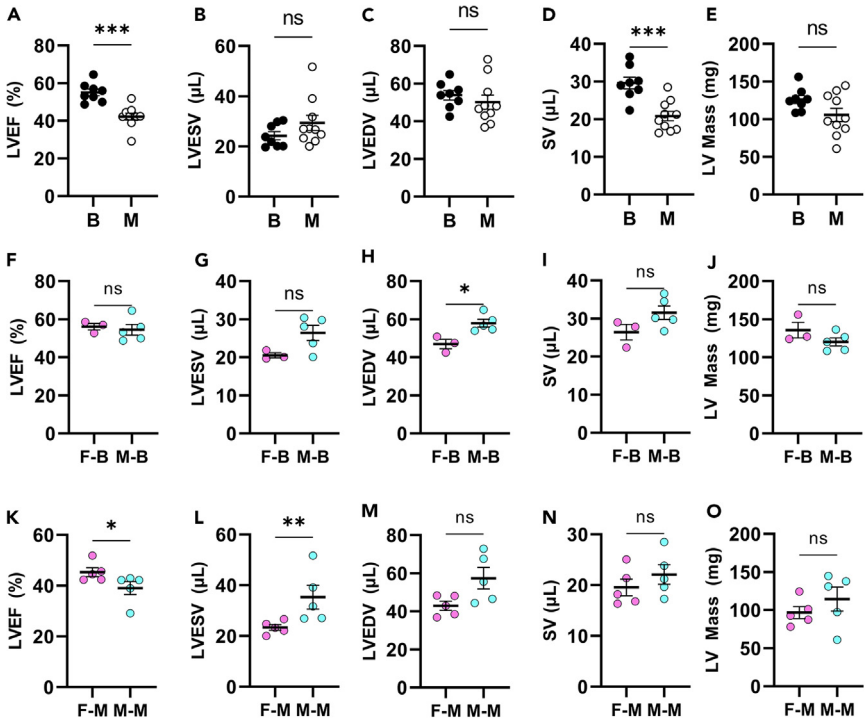

Figure 6. 4D strain software reveals decreased cardiac function during myocarditis in males

(A–E) LV functional parameters from 4D strain software analysis compare baseline (B, n = 8) and myocarditis (M, n = 10) (Mann-Whitney); (F–J) compare females (F-C, n = 3) vs. males (M-B, n = 5) at baseline (Mann-Whitney); (K–O) compare females (F-M, n = 5) vs. males (M-M, n = 5) during myocarditis (Mann-Whitney). Abbreviations: LV, left ventricular; LVEDV, LV end diastolic volume; LVEF, LV ejection fraction; LVESV, LV end systolic volume; SV, stroke volume (scatterplots show mean ± SEM). (A–O) *p < 0.05, **p < 0.01, ***p < 0.001.

mice with myocarditis had a significantly decreased LVEF of 42.4% (p = 0.0002) compared to a baseline of 54.6% (Figure 6A). Stroke volume was significantly decreased with myocarditis compared to baseline (p = 0.0009) (Figure 6B).

Next, we examined the same parameters for males and females at baseline and during myocarditis. At baseline, males had higher LVEDV than females (p = 0.04), but no other sex differences using 4D-mode (Figures 6F–6J). During myocarditis, males had worse LVEF (p = 0.03) (Figure 6K) and a higher LV end systolic volume (LVESV) (p = 0.008) (Figure 6O) than females, indicating worse cardiac function in males. Representative images of baseline and myocarditis changes in LV wall circumference, radial displacement, and LAX position throughout the contraction cycle can be found in Videos S1 and S2.

4D strain reveals worse circumferential strain during myocarditis and in males

The 4D strain software outputs circumferential strain (CS) (the movement of the walls around the SAX of the ventricle) as its primary measure of cardiac strain. Using the 4D Strain software, we found that global CS (GCS) was worse in mice during myocarditis compared to baseline (p = 0.0003) (Figure 7A). We examined CS by region of the LV at the base (top near atria), middle (mid), and apex (bottom tip). We found that CS was worse for each region of the myocardium during myocarditis compared to baseline: base CS (p = 0.0002), mid CS (p < 0.0001), apex CS (p = 0.0002) (Figures 7B–7D). When we examined baseline CS comparing males and females, we found no significant differences in CS for any region. During myocarditis, we found that males had worse CS for all parameters except two that were close to significant, GCS (p = 0.056), mid CS (p = 0.08), base (p = 0.02), and apical (p = 0.03) compared to females (Figures 7J–7M). Bullseye plots and representative 3D renderings of transmural strain demonstrate that radial wall motion decreased overall during myocarditis but is most preserved at the mid-LV (Figure 7E).

2D long-axis strain reveals worse GLS during myocarditis and in males

In this analysis we examined longitudinal contraction/shortening which is quantified using GLS. Using 2D strain software, we found that GLS was worse in mice with myocarditis (−14.48%) compared to baseline (−20.04%) (p < 0.0001) (Figure 8A). A GLS of −20% is considered normal cardiac function, a value of −17% is borderline dysfunction and any value worse than that (closer to 0) indicates decreased function.[4,5] Assessment of traditional echocardiography parameters using the 2D GLS VevoStrain software found that LVEF was significantly decreased during myocarditis (54.73% vs. 43.48%) (p < 0.0001) (Figure 8B), indicating heart failure; LVESV (p = 0.017), LVEDV (p < 0.034), fractional shortening

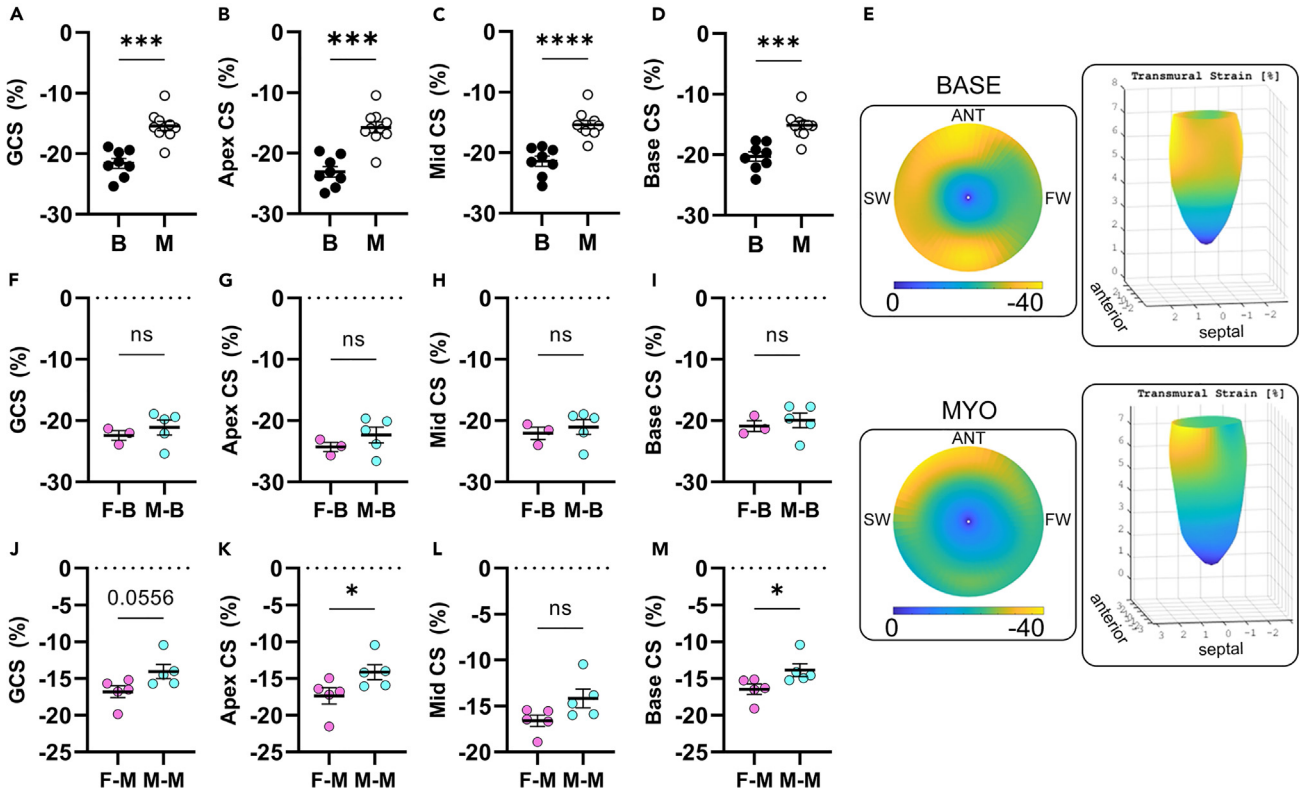

Figure 7. 4D GCS reveals decreased cardiac function during myocarditis in males

(A–D) GCS and CS compare baseline (B, n = 8) vs. myocarditis (M, n = 10) (Mann-Whitney); (F–I) compare females (F-C, n = 3) vs. males (M-B, n = 5) at baseline (Mann-Whitney); (J–M) compare females (F-M, n = 5) vs. males (M-M, n = 5) during myocarditis (Mann-Whitney) (scatterplots show mean ± SEM), (E) representative images show transmural strain with bullseye plots and 3D renderings at peak strain for baseline (BASE) and during myocarditis (MYO). Abbreviations: ANT, anterior wall; CS, regional circumferential strain; FW, free wall; GCS, global circumferential strain; SW, septal wall. (A–M) *p < 0.05, ***p < 0.001, ****p < 0.0001.

(p < 0.0001), stroke volume (p < 0.0001), and CO (p < 0.0001) were worse during myocarditis vs. baseline (Figures 8D–8G). We found that GLS was significantly worse in males (−13.3%) compared to females (−15.86%) with myocarditis (p = 0.019) (Figure 8O). Representative images of endocardial longitudinal strain throughout 3 contraction cycles can be found in Figure 9.

Worse cardiac function by 2D GLS correlates to more severe myocarditis

To determine whether there was a relationship between cardiac inflammation severity and type during myocarditis, we examined the relationship between GLS and cardiac inflammation. We found a significant correlation between worse cardiac function by 2D GLS and myocarditis assessed by H&E (Figure 10A), and immunohistochemistry (IHC) measures of CD45 (Figure 10B), CD11b (Figure 10C), and CD3 (Figure 10E). We observed a similar trend for males for CD11b and CD3. These data suggest that worse cardiac function may relate to the severity of cardiac inflammation.

DISCUSSION

It is important to choose animal models that display high similarities to clinically observed phenotypes to better understand the mechanisms of disease and develop new biomarkers and therapies for disease. The animal model used in this study is highly translational for human myocarditis,[17,21,25,27] which is confirmed in this study by its similarities to echocardiography-derived measures like LVEF and GLS in patients with myocarditis.

Short axis M-mode from the LV is frequently used to measure cardiac dysfunction in animal models of myocarditis where it is good at detecting wall thicknesses and dilation (LVESD, LVEDD). However, M-mode may lack precision for LVEF because it captures a single plane that is less likely to represent the overall movement of the LV wall. Volume-based parameters like LVEF are more accurately assessed using a volume-based measure like 4D mode or 4D strain in rodents and 3D echocardiography in humans (which is equivalent to 4D in rodents).[37–39] In this study, we found that the only echocardiography modes that detected reduced LVEF during myocarditis vs. controls were 2D & 4D strain and 4D Mode (Table 2). Likewise, 2D and 4D strain echocardiography modes found that GLS and GCS were worse during myocarditis compared

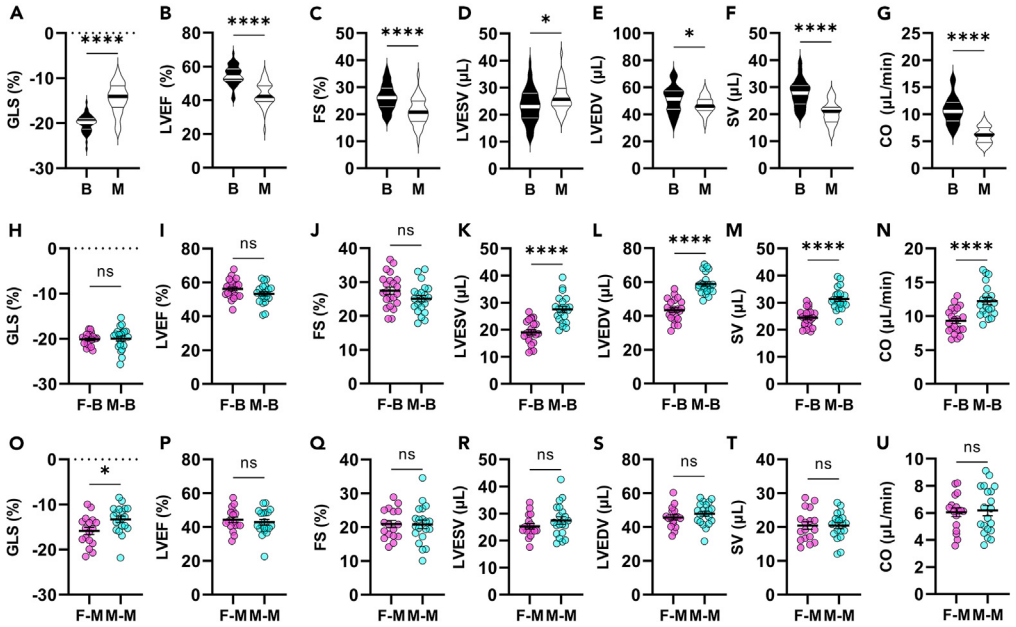

Figure 8. 2D LAX strain reveals worse GLS in myocarditis in males

(A–G) LV functional parameters from 2D LAX strain analysis compare baseline (B, n = 43) and myocarditis (M, n = 37) (unpaired t-test; violin plots depict mean and interquartile range); (H–N) Compare females (F-B, n = 22) vs. males (M-B, n = 21) at baseline (Mann-Whitney); (O–U) Compare females (F-M, n = 17) vs. males (M-M, n = 20) during myocarditis (Mann-Whitney) (scatterplots show mean ± SEM). Abbreviations: CO, cardiac output; FS, fractional shortening; GLS, global longitudinal strain; LV, left ventricular; LVEDV, LV end diastolic volume, LVEF, LV ejection fraction; LVESV, LV end systolic volume; SV, stroke volume. (A–U) *p < 0.05, **p < 0.01, ****p < 0.0001.

to controls and worse in males with myocarditis compared to females. Importantly, males had a larger drop in SV and CO than females comparing baseline to myocarditis (Figure 11). Overall, our data indicate that 2D and 4D strain are the best measure of cardiac dysfunction during viral myocarditis and for detecting sex differences during myocarditis.

The 4D Strain Toolbox was created by Dr. Craig Goergen's laboratory at Purdue University, works in combination with the VisualSonics Vevo LAB software to create 4D contours in a single cardiac cycle.[40,41] In this study we found that mice with myocarditis had worse GCS compared to mice at baseline, which was characterized by decreased CS at the base, mid-LV and apex (Figure 7). Representative images

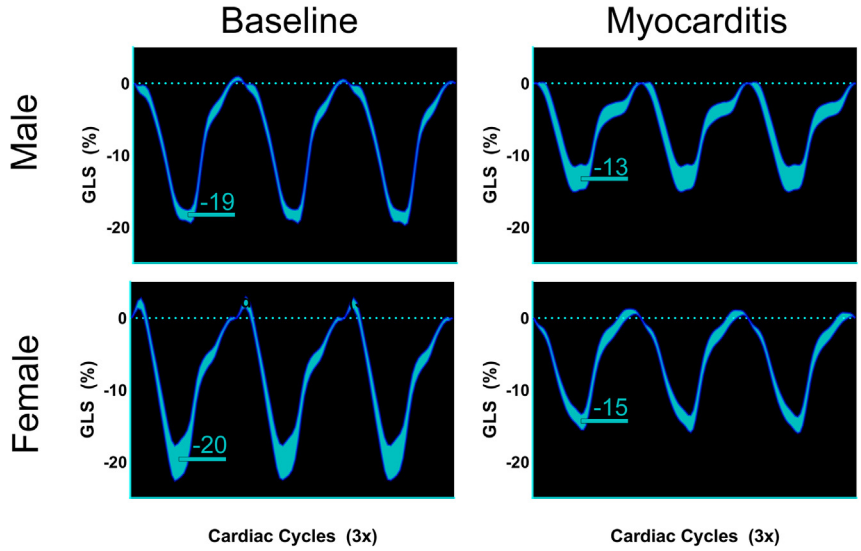

Figure 9. Representative 2D long axis strain images

Representative images showing endocardial global longitudinal strain (GLS) (mean ± 95% confidence intervals) among 3 contraction cycles of female and male mice at baseline and during myocarditis.

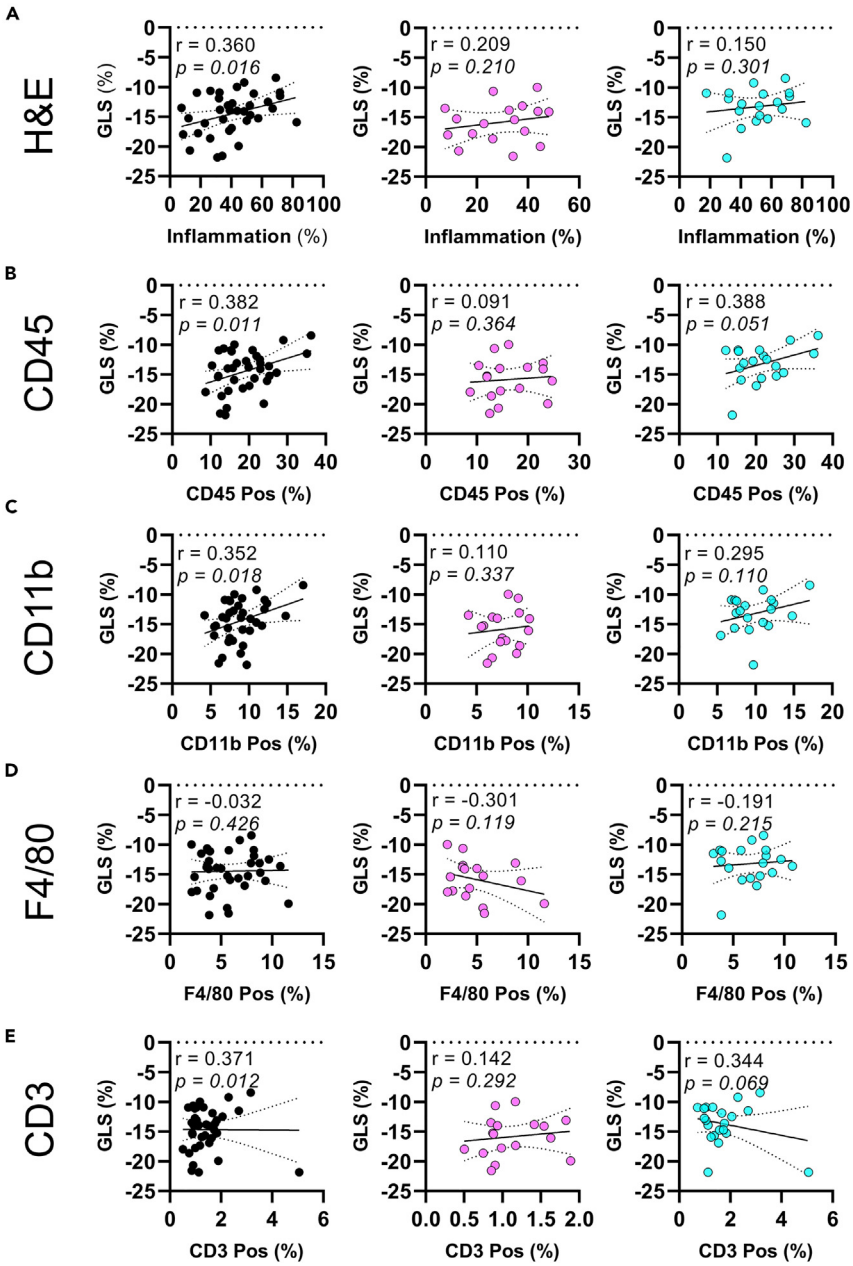

Figure 10. GLS correlates to CD11b and CD3 inflammation

Global longitudinal strain (GLS) correlation to (A) H&E score, or immunohistochemistry for (B) CD45; (C) CD11b; (D) F4/80; or (E) CD3 during myocarditis. **Black**, females and males, **pink**, females only, **turquoise**, males only. Data are represented as linear regressions with one-way Pearson correlations.

and videos of baseline and myocarditis transmural strain show that radial movement is somewhat preserved at the mid-LV and at the base of the heart along the posterior side (Figure 7, Videos S1 and S2). We suspect the differences in LVEF between short axis M-mode (Figure 4, Table 1) vs. other imaging modes in our dataset (Table 2) are due to radial contractile preservation at the mid-LV during myocarditis and biased sampling at this region due to a single plane short axis image.

Because of drawbacks with echocardiography to describe cardiac dysfunction during myocarditis, GLS is increasingly being used in the clinical setting. Most studies have shown that patients with myocarditis have GLS values in the −17 to −10 range, representing acutely impaired longitudinal ventricular shortening.[4,5,42] One study found that a value of −14 or worse (closer to 0) was significantly associated with major adverse cardiac events and all-cause mortality in a cohort of 101 patients with myocarditis.[42] Our findings demonstrate GLS in a similar range to those observed in the literature (Figure 8). Importantly, GLS was able to detect sex differences in cardiac function during

Table 2. Left-ventricular parameters compared across techniques: baseline versus myocarditis

	Mean ± SEM[a]									
	LVEF		LVESV		LVEDV		SV		CO	
Parameter	B	M	B	M	B	M	B	M	B	M
SAX M-Mode	53.24[b] (1.18)	50.02 (1.42)	32.44 (1.32)	31.17 (1.18)	68.54 (1.44)	**64.22***[c] (1.44)	36.11 (0.81)	**32.05*** (1.13)	13.36 (0.41)	**9.36*** (0.42)
4D Mode	51.94 (1.46)	**43.87*** (1.86)	19.89 (0.91)	**20.71*** (1.47)	41.48 (1.49)	**36.85*** (2.09)	21.59 (0.99)	**16.14*** (1.10)	7.97 (0.46)	**4.28*** (0.36)
4D Strain	55.08 (1.80)	**42.22*** (1.80)	24.22 (1.61)	29.33 (3.01)	53.83 (2.47)	50.16 (3.76)	29.61 (1.57)	**20.83*** (1.26)	– –	– –
2D LAX Strain	54.73 (0.89)	**43.48*** (1.17)	23.19 (0.96)	**26.42*** (0.88)	50.98 (1.52)	**46.85*** (1.06)	27.79 (0.77)	**20.43*** (0.70)	10.72 (0.39)	**6.11*** (0.25)

[a]B, baseline; CO, cardiac output; LVEF, left ventricular ejection fraction; LVEDV, left ventricular end diastolic volume; LVESV, left ventricular end systolic volume; M, myocarditis; SEM, standard error of the mean; SV, stroke volume; *, $p < 0.050$ comparing baseline to myocarditis.
[b]Data are represented as mean ± SEM.
[c]Bolded p values indicate statistical significance for unpaired t-test.

myocarditis with males displaying worse function (Figure 8). Thus, we show in this manuscript that GLS differs by sex in a mouse model of myocarditis and cardiac function is related to CD11b infiltrate (Figure 10).

Based on our findings we recommend that future echocardiography studies of mouse models that use M-mode should include a representative M-mode image and a representative image of the short axis plane from which the M-mode was acquired to improve transparency of imaging. Investigators should consider utilizing a 4D imaging mode to limit estimation of volume from a single plane. If 4D mode is not available, volume-based measurements using estimates from single plane images should be obtained from the longitudinal axis of the LV and analyzed via 2D strain which most closely resembles our finding with 4D-mode and 4D strain (Table 2). In conclusion, our findings indicate that 2D and 4D strains were the best indicators of cardiac dysfunction using echocardiography in a mouse model of viral myocarditis finding reduced function during disease compared to baseline and identifying sex differences in disease.

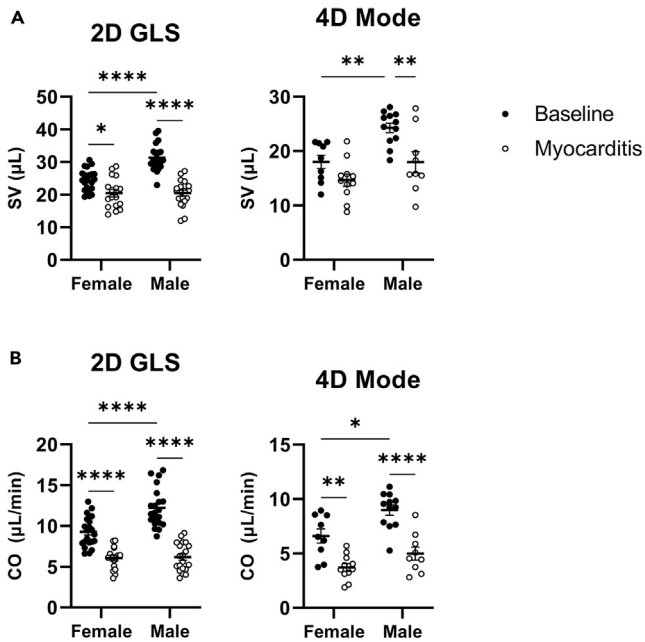

Figure 11. Greater reduction in cardiac function in males during myocarditis

(A) Sex differences in stroke volume as measured by 2D GLS software and 4D mode (two-way ANOVA mixed effects model with Tukey's multiple comparisons)
(B) Sex differences in cardiac output as measured by 2D GLS software and 4D mode (two-way ANOVA mixed effects model with Tukey's multiple comparisons; scatterplots show mean ± SEM). Abbreviations: CO; cardiac output, GLS; global longitudinal strain, SV; stroke volume. (A–B) *$p < 0.05$, **$p < 0.01$, ****$p < 0.0001$.

Limitations of the study

A primary limitation of our analysis is the reduced sample size for 4D imaging modes leaving the potential for selection bias; in brief, due to time and image quality limitations, only the highest quality images were used for analysis. The quality of 4D images was determined by the sonographer who viewed 4D images in motion from longitudinal and short axis in motion. Samples with uneven image alignment or artifacts on serial short-axis images that would prevent accurate analysis were excluded. For 4D strain, only a small subset of high-quality images was used. For 4D and 2D strain, images were excluded if the software tracking wall movement did not represent the movement of the wall (i.e., artifacts prevent speckle-tracking). One sample from males with myocarditis was excluded due to non-optimal sectioning which seemed to bias the sample toward a higher histology score. Additionally, our experience with isoflurane anesthesia (in this and other cardiac dysfunction models) has demonstrated that prolonged exposure may alter the immune response; however, this was controlled for since all echocardiography data were obtained from mice with the same level of exposure. Although the purpose of this study was to examine echocardiography modalities for their ability to detect sex differences in myocarditis, the analysis would have been improved by comparing echocardiography-derived GLS to measures obtained from CMR or pressure-volume loop analysis. However, this equipment was not available at our institution.

STAR★METHODS

Detailed methods are provided in the online version of this paper and include the following:

- KEY RESOURCES TABLE
- RESOURCE AVAILABILITY
  - Lead contact information
  - Materials availability
  - Data and code availability
- EXPERIMENTAL MODEL AND ANIMAL CARE DETAILS
  - Animal care ethics statement
  - CVB3-induced Myocarditis Model
- METHOD DETAILS
  - Histology
  - Immunohistochemistry
  - Echocardiography
- QUANTIFICATION AND STATISTICAL ANALYSIS
  - Statistical analysis

SUPPLEMENTAL INFORMATION

Supplemental information can be found online at https://doi.org/10.1016/j.isci.2023.108493.

ACKNOWLEDGMENTS

The authors would like to thank the Dennis Dickson Histology Group for their work embedding and staining slides for this project. This group includes Dennis W. Dickson, PhD, Linda Rousseau, Virginia Phillips, Ariston Libraro, and Monica Castanedes. The Cardiovascular Imaging Research Laboratory at Purdue University under the guidance of Dr. Craig Goergen and in collaboration with FUJIFILM VisualSonics, imagined, developed, validated the 4DUS Strain Toolbox. The rights of invention have been assigned to the Purdue Research Foundation. The use of the 4D Strain Toolbox was a generous loan of Purdue University, in collaboration with FUJIFILM VisualSonics. This work was supported by National Institutes of Health (NIH) R01 HL164520, R21 AI145356, R21 AI152318, R21 AI154927 to D.F.; and American Heart Association 20TPA35490415 to D.F.; NIH grants UL1 TR002377 to D.N.D., D.J.B., E.R.W., D.F.; TL1 TR002380 to D.N.D., D.J.B., E.R.W.; R21 AI163302 to K.A.B.; R01 HL135165 to L.T.C.; and Mayo Clinic Center for Regenerative Medicine to D.F.

AUTHOR CONTRIBUTIONS

Conceptualization: D.N.D., D.J.B., L.P.M., S.K.B., L.J.R., K.A.B., and D.F. data acquisition: D.N.D., D.J.B., L.P.M., N.B.H., A.N.N., S.K., P.G.G., G.J.B., V.B., S.K.B., and L.J.R. sample acquisition: D.N.D., N.B.H., S.K., E.R.W., P.G.G., B.H.E., and V.B. methodology: D.N.D., D.N.B., L.P.M., B.H.E., S.K.B., and L.J.R. data analysis: D.N.D., K.A.S., D.J.B., P.G.G., G.J.W., L.T.C., C.K.L., and D.F. data curation: D.N.D., D.J.B., K.A.S., and V.B. project administration: D.N.D., and D.F. writing - original draft: D.N.D., D.J.B., and D.F.

DECLARATION OF INTERESTS

The authors declare no conflict of interest.

INCLUSION AND DIVERSITY

We support inclusive, diverse, and equitable conduct of research.

Received: May 30, 2023
Revised: October 2, 2023
Accepted: November 16, 2023
Published: November 20, 2023

REFERENCES

1. Richardson, P., McKenna, W., Bristow, M., Maisch, B., Mautner, B., O'Connell, J., Olsen, E., Thiene, G., Goodwin, J., Gyarfas, I., et al. (1996). Report of the 1995 World Health Organization/International Society and Federation of Cardiology Task Force on the Definition and Classification of cardiomyopathies. Circulation *93*, 841–842.
2. Risgaard, B., Winkel, B.G., Jabbari, R., Behr, E.R., Ingemann-Hansen, O., Thomsen, J.L., Ottesen, G.L., Gislason, G.H., Bundgaard, H., Haunsø, S., et al. (2014). Burden of sudden cardiac death in persons aged 1 to 49 years: nationwide study in Denmark. Circ. Arrhythm. Electrophysiol. *7*, 205–211.
3. Tschöpe, C., Ammirati, E., Bozkurt, B., Caforio, A.L.P., Cooper, L.T., Felix, S.B., Hare, J.M., Heidecker, B., Heymans, S., Hübner, N., et al. (2021). Myocarditis and inflammatory cardiomyopathy: current evidence and future directions. Nat. Rev. Cardiol. *18*, 169–193.
4. Doimo, S., Ricci, F., Aung, N., Cooper, J., Boubertakh, R., Sanghvi, M.M., Sinagra, G., and Petersen, S.E. (2020). Tissue-tracking in the assessment of late gadolinium enhancement in myocarditis and myocardial infarction. Magn. Reson. Imaging *73*, 62–69.
5. Weckbach, L.T., Curta, A., Bieber, S., Kraechan, A., Brado, J., Hellmuth, J.C., Muenchhoff, M., Scherer, C., Schroeder, I., Irlbeck, M., et al. (2021). Myocardial inflammation and dysfunction in COVID-19-associated myocardial injury. Circ. Cardiovasc. Imaging *14*, e012220.
6. Patel, Y.R., Louis, D.W., Atalay, M., Agarwal, S., and Shah, N.R. (2021). Cardiovascular magnetic resonance findings in young adult patients with acute myocarditis following mRNA COVID-19 vaccination: a case series. J. Cardiovasc. Magn. Reson. *23*, 101.
7. Fischer, K., Linder, O.L., Erne, S.A., Stark, A.W., Obrist, S.J., Bernhard, B., Guensch, D.P., Huber, A.T., Kwong, R.Y., and Gräni, C. (2022). Reproducibility and its confounders of CMR feature tracking myocardial strain analysis in patients with suspected myocarditis. Eur. Radiol. *32*, 3436–3446.
8. Isaak, A., Kravchenko, D., Mesropyan, N., Endler, C., Bischoff, L.M., Vollbrecht, T., Thomas, D., Dabir, D., Zimmer, S., Attenberger, U., et al. (2022). Layer-specific strain analysis with cardiac MRI feature tracking in acute myocarditis. Radiol. Cardiothorac. Imaging *4*, e210318.
9. Vos, J.L., Raafs, A.G., van der Velde, N., Germans, T., Biesbroek, P.S., Roes, K., Hirsch, A., Heymans, S.R.B., and Nijveldt, R. (2022). Comprehensive cardiovascular magnetic resonance-derived myocardial strain analysis provides independent prognostic value in acute myocarditis. J. Am. Heart Assoc. *11*, e025106.
10. Luetkens, J.A., Petry, P., Kuetting, D., Dabir, D., Schmeel, F.C., Homsi, R., Schild, H.H., and Thomas, D. (2018). Left and right ventricular strain in the course of acute myocarditis: a cardiovascular magnetic resonance study. Röfo *190*, 722–732.
11. Cruz-Adalia, A., Jiménez-Borreguero, L.J., Ramírez-Huesca, M., Chico-Calero, I., Barreiro, O., López-Conesa, E., Fresno, M., Sánchez-Madrid, F., and Martín, P. (2010). CD69 limits the severity of cardiomyopathy after autoimmune myocarditis. Circulation *122*, 1396–1404.
12. Gorelik, M., Lee, Y., Abe, M., Andrews, T., Davis, L., Patterson, J., Chen, S., Crother, T.R., Aune, G.J., Noval Rivas, M., and Arditi, M. (2019). IL-1 receptor antagonist, anakinra, prevents myocardial dysfunction in a mouse model of Kawasaki disease vasculitis and myocarditis. Clin. Exp. Immunol. *198*, 101–110.
13. Roth, G.A., Mensah, G.A., Johnson, C.O., Addolorato, G., Ammirati, E., Baddour, L.M., Barengo, N.C., Beaton, A.Z., Benjamin, E.J., Benziger, C.P., et al. (2020). Global burden of cardiovascular diseases and risk factors, 1990-2019: update from the GBD 2019 Study. J. Am. Coll. Cardiol. *76*, 2982–3021.
14. Fairweather, D., Beetler, D.J., Musigk, N., Heidecker, B., Lyle, M.A., Cooper, L.T., Jr., and Bruno, K.A. (2023). Sex and gender differences in myocarditis and dilated cardiomyopathy: an update. Front. Cardiovasc. Med. *10*, 1129348.
15. Kytö, V., Sipilä, J., and Rautava, P. (2013). The effects of gender and age on occurrence of clinically suspected myocarditis in adulthood. Heart *99*, 1681–1684.
16. Laufer-Perl, M., Havakuk, O., Shacham, Y., Steinvil, A., Letourneau-Shesaf, S., Chorin, E., Keren, G., and Arbel, Y. (2017). Sex-based differences in prevalence and clinical presentation among pericarditis and myopericarditis patients. Am. J. Emerg. Med. *35*, 201–205.
17. Coronado, M.J., Bruno, K.A., Blauwet, L.A., Tschöpe, C., Cunningham, M.W., Pankuweit, S., van Linthout, S., Jeon, E.S., McNamara, D.M., Krejčí, J., et al. (2019). Elevated sera sST2 is associated with heart failure in men ≤ 50 years old with myocarditis. J. Am. Heart Assoc. *8*, e008968.
18. Lynge, T.H., Nielsen, T.S., Gregers Winkel, B., Tfelt-Hansen, J., and Banner, J. (2019). Sudden cardiac death caused by myocarditis in persons aged 1-49 years: a nationwide study of 14 294 deaths in Denmark. Forensic Sci. Res. *4*, 247–256.
19. Wong, B.T.W., and Christiansen, J.P. (2020). Clinical characteristics and prognostic factors of myocarditis in New Zealand patients. Heart Lung Circ. *29*, 1139–1145.
20. Ozierański, K., Tymińska, A., Kruk, M., Koń, B., Skwarek, A., Opolski, G., and Grabowski, M. (2021). Occurrence, trends, management and outcomes of patients hospitalized with clinically suspected myocarditis-ten-year perspectives from the MYO-PL Nationwide Database. J. Clin. Med. *10*, 4672.
21. Fairweather, D., Kaya, Z., Shellam, G.R., Lawson, C.M., and Rose, N.R. (2001). From infection to autoimmunity. J. Autoimmun. *16*, 175–186.
22. Frisancho-Kiss, S., Nyland, J.F., Davis, S.E., Frisancho, J.A., Barrett, M.A., Rose, N.R., and Fairweather, D. (2006). Sex differences in coxsackievirus B3-induced myocarditis: IL-12Rbeta1 signaling and IFN-gamma increase inflammation in males independent from STAT4. Brain Res. *1126*, 139–147.
23. Frisancho-Kiss, S., Davis, S.E., Nyland, J.F., Frisancho, J.A., Cihakova, D., Barrett, M.A., Rose, N.R., and Fairweather, D. (2007). Cutting Edge: Cross-regulation by TLR4 and T cell Ig mucin-3 determines sex differences in inflammatory heart disease. J. Immunol. *178*, 6710–6714.
24. Fairweather, D., Cooper, L.T., Jr., and Blauwet, L.A. (2013). Sex and gender differences in myocarditis and dilated cardiomyopathy. Curr. Probl. Cardiol. *38*, 7–46.
25. Heidecker, B., Dagan, N., Balicer, R., Eriksson, U., Rosano, G., Coats, A., Tschöpe, C., Kelle, S., Poland, G.A., Frustaci, A., et al. (2022). Myocarditis following COVID-19 vaccine: incidence, presentation, diagnosis, pathophysiology, therapy, and outcomes put into perspective. A clinical consensus document supported by the Heart Failure Association of the European Society of Cardiology (ESC) and the ESC Working Group on Myocardial and Pericardial Diseases. Eur. J. Heart Fail. *24*, 2000–2018.
26. Kottwitz, J., Bruno, K.A., Berg, J., Salomon, G.R., Fairweather, D., Elhassan, M., Baltensperger, N., Kissel, C.K., Lovrinovic, M., Baltensweiler, A., et al. (2020). Myoglobin for detection of high-risk patients with acute myocarditis. J. Cardiovasc. Transl. Res. *13*, 853–863.
27. Blanco-Domínguez, R., Sánchez-Díaz, R., de la Fuente, H., Jiménez-Borreguero, L.J., Matesanz-Marín, A., Relaño, M., Jiménez-Alejandre, R., Linillos-Pradillo, B., Tsilingiri, K., Martín-Mariscal, M.L., et al. (2021). A novel circulating microRNA for the detection of acute myocarditis. N. Engl. J. Med. *384*, 2014–2027.
28. Beetler, D.J., Bruno, K.A., Di Florio, D.N., Douglass, E.J., Shrestha, S., Tschöpe, C., Cunningham, M.W., Krejčí, J., Bienertová-Vašků, J., Pankuweit, S., et al. (2022). Sex and age differences in sST2 in cardiovascular disease. Front. Cardiovasc. Med. *9*, 1073814.
29. Fairweather, D., Frisancho-Kiss, S., Njoku, D.B., Nyland, J.F., Kaya, Z., Yusung, S.A., Davis, S.E., Frisancho, J.A., Barrett, M.A., and Rose, N.R. (2006). Complement receptor 1 and 2 deficiency increases coxsackievirus B3-induced myocarditis, dilated

cardiomyopathy, and heart failure by increasing macrophages, IL-1beta, and immune complex deposition in the heart. J. Immunol. *176*, 3516–3524.

30. Fairweather, D., Coronado, M.J., Garton, A.E., Dziedzic, J.L., Bucek, A., Cooper, L.T., Jr., Brandt, J.E., Alikhan, F.S., Wang, H., Endres, C.J., et al. (2014). Sex differences in translocator protein 18 kDa (TSPO) in the heart: implications for imaging myocardial inflammation. J. Cardiovasc. Transl. Res. *7*, 192–202.
31. Cooper, L.T., Jr., Onuma, O.K., Sagar, S., Oberg, A.L., Mahoney, D.W., Asmann, Y.W., and Liu, P. (2010). Genomic and proteomic analysis of myocarditis and dilated cardiomyopathy. Heart Fail. Clin. *6*, 75–85.
32. Satoh, M., Nakamura, M., Akatsu, T., Iwasaka, J., Shimoda, Y., Segawa, I., and Hiramori, K. (2003). Expression of Toll-like receptor 4 is associated with enteroviral replication in human myocarditis. Clin. Sci. *104*, 577–584.
33. Satoh, M., Nakamura, M., Akatsu, T., Shimoda, Y., Segawa, I., and Hiramori, K. (2004). Toll-like receptor 4 is expressed with enteroviral replication in myocardium from patients with dilated cardiomyopathy. Lab. Invest. *84*, 173–181.
34. Fairweather, D., Yusung, S., Frisancho, S., Barrett, M., Gatewood, S., Steele, R., and Rose, N.R. (2003). IL-12 receptor beta 1 and Toll-like receptor 4 increase IL-1 beta- and IL-18-associated myocarditis and coxsackievirus replication. J. Immunol. *170*, 4731–4737.
35. Pappritz, K., Lin, J., El-Shafeey, M., Fechner, H., Kühl, U., Alogna, A., Spillmann, F., Elsanhoury, A., Schulz, R., Tschöpe, C., and Van Linthout, S. (2022). Colchicine prevents disease progression in viral myocarditis via modulating the NLRP3 inflammasome in the cardiosplenic axis. ESC Heart Fail. *9*, 925–941.
36. Myers, J.M., Cooper, L.T., Kem, D.C., Stavrakis, S., Kosanke, S.D., Shevach, E.M., Fairweather, D., Stoner, J.A., Cox, C.J., and Cunningham, M.W. (2016). Cardiac myosin-Th17 responses promote heart failure in human myocarditis. JCI Insight *1*, e85851.
37. Caiani, E.G., Sugeng, L., Weinert, L., Capderou, A., Lang, R.M., and Vaïda, P. (2006). Objective evaluation of changes in left ventricular and atrial volumes during parabolic flight using real-time three-dimensional echocardiography. J. Appl. Physiol. (1985) *101*, 460–468.
38. Tsang, W., and Lang, R.M. (2013). Three-dimensional echocardiography is essential for intraoperative assessment of mitral regurgitation. Circulation *128*, 643–652. discussion 652.
39. Poon, J., Leung, J.T., and Leung, D.Y. (2019). 3D echo in routine clinical practice - state of the art in 2019. Heart Lung Circ. *28*, 1400–1410.
40. Damen, F.W., Salvas, J.P., Pereyra, A.S., Ellis, J.M., and Goergen, C.J. (2021). Improving characterization of hypertrophy-induced murine cardiac dysfunction using four-dimensional ultrasound-derived strain mapping. Am. J. Physiol. Heart Circ. Physiol. *321*, H197–H207.
41. Damen, F.W., Newton, D.T., Lin, G., and Goergen, C.J. (2021). Machine learning driven contouring of high-frequency four-dimensional cardiac ultrasound data. Appl. Sci. *11*, 1690.
42. Awadalla, M., Mahmood, S.S., Groarke, J.D., Hassan, M.Z.O., Nohria, A., Rokicki, A., Murphy, S.P., Mercaldo, N.D., Zhang, L., Zlotoff, D.A., et al. (2020). Global longitudinal strain and cardiac events in patients with immune checkpoint inhibitor-related myocarditis. J. Am. Coll. Cardiol. *75*, 467–478.
43. Myers, J.M., Fairweather, D., Huber, S.A., and Cunningham, M.W. (2013). Autoimmune myocarditis, valvulitis, and cardiomyopathy. Curr Protoc Immunol *Chapter*. Curr. Protoc. Immunol. *1*. Chapter 15, Unit 15.14.1-51.
44. Abston, E.D., Coronado, M.J., Bucek, A., Onyimba, J.A., Brandt, J.E., Frisancho, J.A., Kim, E., Bedja, D., Sung, Y.K., Radtke, A.J., et al. (2013). TLR3 deficiency induces chronic inflammatory cardiomyopathy in resistant mice following coxsackievirus B3 infection: role for IL-4. Am. J. Physiol. Regul. Integr. Comp. Physiol. *304*, R267–R277.

STAR★METHODS

KEY RESOURCES TABLE

REAGENT or RESOURCE	SOURCE	IDENTIFIER
Antibodies		
CD45	Biolegend	103102
CD11b	Abcam	Ab133357
CD3	Abcam	Ab16669
F4/80	BioRad	MCA497G
Anti-rabbit labeled polymer	Envision +	K4003
Bacterial and virus strains		
Coxsackievirus B3 Nancy Strain	ATCC	VR-30
Critical commercial assays		
Rat on Rodent Kit	Biocare	RT517
Experimental models: Cell lines		
Vero Cells	ATCC	CCL-81
Experimental models: Organisms/strains		
Mice: 6–8 week old BALB/c WT	Jackson Labs	651
Software and algorithms		
Vevo Lab	Visual Sonics	
4D Strain	Purdue University	
Prism V9-10	GraphPad	
Deposited data		
Dataset for Sex Diff in Echo	This paper	https://doi.org/10.5061/dryad.mcvdnck6f

RESOURCE AVAILABILITY

Lead contact information

- Information and requests for resources should be directed to Dr. DeLisa Fairweather (Fairweather.DeLisa@mayo.edu).

Materials availability

- This study did not generate new unique reagents.

Data and code availability

- This manuscript did not utilize or report original code.
- The original data for this manuscript is available from Dryad (iSci_52623; https://doi.org/10.5061/dryad.mcvdnck6f)
- Any additional information required to reanalyze the data reported in this paper is available from the lead contact upon request.

EXPERIMENTAL MODEL AND ANIMAL CARE DETAILS

Animal care ethics statement

Mice were used in strict accordance with the recommendations in the Guide for the Care and Use the Laboratory Animals of the National Institutes of Health (NIH) and approval obtained from the Animal Care and Use Committee at Mayo Clinic Florida for all procedures (IACUC# A00003984). Mice were maintained under pathogen-free conditions in the animal facility at Mayo Clinic Florida and mice were sacrificed according to the Guide for the Care and Use of Laboratory Animals of the NIH.

CVB3-induced Myocarditis Model

Male BALB/cJ (strain #000651) 7 to 8-week-old adult mice were obtained from the Jackson Laboratory (Bar Harbor, ME). Mice were maintained under pathogen-free conditions in the animal facility at the Mayo Clinic Florida. Mice were inoculated intraperitoneally (ip) with 10^3

plaque forming units (PFU) of heart-passaged stock of CVB3 on day 0, and myocarditis examined at day 10 post infection (pi).[29,30] CVB3 (Nancy strain) was obtained from the American Type Culture Collection (ATCC; Manassas, VA) and grown in Vero cells (ATCC) to create a tissue culture-derived virus stock.[43] 100 μL of tissue culture virus (10^3 PFU) was injected ip into 4 week old female BALB/c mice and virus obtained from hearts at day 3 pi by homogenization in Gibco Minimum Essential Media (Thermo-Scientific, Waltham, MA, 11095-080) supplemented with 2% heat inactivated FBS.[43] Homogenized hearts were centrifuged at 4C for 20 min at 795*g*. Homogenized supernatant that contains infectious virus and damaged heart proteins (heart-passaged virus) was stored at −80 until used to induce myocarditis.[43]

METHOD DETAILS

Histology

Mouse hearts were cut longitudinally and fixed in 10% phosphate-buffered formalin and embedded in paraffin for histological analysis. 5 μm sections were stained with hematoxylin and eosin (H&E) to detect inflammation. Myocarditis was assessed as the percentage of the heart with inflammation compared to the overall size of the heart section using a microscope eyepiece grid.[22,30,34] Sections were scored by at least two individuals blinded to the treatment group. One sample from males with myocarditis was excluded due to non-optimal sectioning which seemed to bias the sample toward a higher inflammation score.

Immunohistochemistry

Heart sections (5 μm) were stained with CD45 (Biolegend, San Diego, CA, 103102, 1:200, rat), CD11b (Abcam, Cambridge, United Kingdom, ab133357, 1:3000, rabbit), CD3 (Abcam, ab16669, 1:200, rabbit), and F4/80 (BioRad, Hercules, CA, MCA497G, 1:250, rat). A Envision+ anti-rabbit labeled polymer (K4003) and rat-on-rodent kit (RT517) (Biocare, Pacheco, CA) were used as secondary antibodies for rat antibodies. Stained slides were scanned using an Aperio AT2 slide scanner (Leica, Wetzlar, Germany). Ventricles of cardiac sections were manually selected by a lab member blinded to the study groups for analysis. The default "positive pixel" algorithm was modified for each stain by adjusting the Color Saturation Threshold so that the program's selection of positive and negative pixel counted accurately reflected each stain. The color saturation thresholds for antibodies are as follows: CD45 0.03, CD11b 0.14, CD3 0.03, F4/80 same as default settings. The hue for all algorithms used was 0.1, brown. The staining of each slide was analyzed using Aperio eSlide Manager (Leica, Wetzlar, Germany) with the aforementioned algorithms. Stain positivity (% positive) for each marker was determined with a "Positivity" parameter (positivity = number of positive pixels/(number of positive + number of negative pixels)), as previously described.[4] Percent positive was used to assess CD3 (number of positive pixels/total pixels). One sample from males with myocarditis was excluded due to non-optimal sectioning which seemed to bias the sample toward a higher histology score.

Echocardiography

Cardiac function was determined by transthoracic echocardiography performed using the Vevo 3100 Ultrasound machine equipped with a MX550D 40 MHz transducer mounted to a "3D Motor" (VisualSonics Inc., Toronto, Canada). Mice were sedated with 3% isoflurane, hair across the abdominal cavity was removed using Nair while isoflurane sedation was continued at 1–3% depending on animal heart rate, and ultrasonic transmission gel (Parker Laboratories, Fairfield, NJ) was applied to the thorax.[17,29,44] Mice received the anesthetic isoflurane on days −5 to −3 prior to infection with coxsackievirus B3 to obtain baseline (B) echocardiography cardiac function assessments and at day 10 during myocarditis (M). While under anesthesia, healthy mice were maintained at a heart rate of 350–450 beats per minute (bpm). Two-dimensional (2D) parasternal long-axis (LAX) and short-axis (SAX) of the left-ventricle (LV) were acquired in B-mode. An M-mode image of the SAX was acquired by positioning the LV posterior wall at the level of the papillary muscles so both the free and septal wall were visible along with a portion of the right ventricle. Using the Vevo 3100 4D image acquisition software with the 3D motor, a cine loop for an entire cardiac cycle was obtained in the SAX plane across the heart. The 4D data were acquired with the VisualSonics Vevo®3100 and analyzed using an alpha version of a 4D Strain Toolbox as described in Damen et al., 2021.[41] 4D data were acquired using the MX550D 40 MHz transducer along the short-axis of the heart at a frame rate of 40 MHz and a step size of 0.1 mm. For this acquisition, SAX images were acquired from below the apex of the heart up to the base of the heart using 100 μm steps for a total scan distance of 8-10 mm (depending on the size of the heart). Collected SAX images were then reconstructed to generate a 3D "cube" view for visualizing the heart anatomy across various planes and 4D strain analysis. The 4D strain software was provided through a collaborative effort with VisualSonics and Dr. Craig J. Goergen at Purdue University as part of an alpha testing trial.

Prior to image analysis, images were checked for quality and poor-quality images excluded. This was important because inaccurate analysis of the LV would affect 4D image analysis and 2D strain. For 2D analysis, the Vevo LAB auto-LV artificial intelligence tool was used to analyze M-mode parameters of 3–5 cardiac cycles and manual adjustments to the artificial intelligence tracing were made when necessary (occurred most often for the anterior epicardial wall). For echocardiography-derived global longitudinal strain (GLS), LAX images were analyzed using Vevo Strain analysis software (within Vevo LAB) with three cardiac cycles. For 4D analysis, after quality control checking 4D images for image alignment, 4D images of the LV were analyzed using Vevo LAB by tracing every 5 SAX images, the volumes were traced 2–3 times and measurements were averaged. 4D strain analysis required more rigorous quality control measures due to the software's need to perform speckle-tracking along both the SAX and LAX; prior to analysis, 4D volumes were assessed as above for 4D mode and for optimal signal/noise. The 4D strain software was on loan for a limited period of time which is why only a minimal subset of the highest quality images were used. 4D strain (circumferential strain) was measured by tracking the movement of the LV endocardial wall only.

Fractional shortening (FS) is the percent change in LV cavity dimensions. Ejection fraction (EF) represents stroke volume (SV) as a percentage of end diastolic LV volume. The heart rate was determined using the built-in electrocardiographic probes in the Vevo Lab's Imaging Station. Cardiac output (CO) is the heart rate times the SV.

All strain measures (2D GLS and 4D global circumferential strain) were derived from the formula for cardiac strain which is defined by the difference in movement of a wall from its starting position at end-diastolic diameter to its end position at end-systolic diameter divided by the original position of the wall. This effectively represents a percent-change in wall position composed of individual component vectors. For 2D LAX this includes the longitudinal and radial movement vectors and for 4D strain this includes the circumferential and longitudinal vectors.

QUANTIFICATION AND STATISTICAL ANALYSIS

Statistical analysis

Statistical analyses were performed using GraphPad Prism 9. Normally distributed data comparing two groups were analyzed using a 2-tailed Student's *t* test. The Mann-Whitney rank-sum test was used to evaluate nonparametric data. Violin plots express data as mean and interquartile range. Scatterplots display data as mean ± SEM. When comparing more than 2 groups multiple comparison analysis was performed by ANOVA (and nonparametric equivalent for nonparametric data) with each group compared to the corresponding control group. Correlations are represented with linear regression and one-way Pearson correlations. A two-way ANOVA with repeated measures was used for Figure 10. Data are expressed as mean ± SEM. A value of $p < 0.05$ was considered significant. Statistical test information is provided in the figure legends. p values are depicted as *$p < 0.05$, **$p < 0.01$, ***$p < 0.001$, ****$p < 0.0001$.